Chapter 7

Particle Identification

The particle identification (PID) in BRAHMS is accomplished by a combination of time-of-flight and Čerenkov detectors. The momentum ranges to be covered in the forward arm and the mid-rapidity arm are different, but the techniques used for particle identification are similar. In both cases the lower K-p range is covered by time-of-flight, and the higher range by Čerenkov detectors. This chapter first gives an overview of the PID scheme in the forward and mid-rapidity arms followed by a more detailed discussion of the TOF design and tests, as well as the RICH detector.

7.1 Forward spectrometer

Particle identification in the forward arm spectrometer is done in two places:

- Between D2 and D3. This is needed for the low momentum part of the spectra where 1 GeV/$c < p \leq 5$ GeV/c in the angular range $2° < \theta < 18°$, and is the only PID for $18° < \theta < 35°$ where the measurements are done by the D1-D2 complex alone.

- After D4. This will cover the high momentum part of the spectra, i.e., $p \geq 5$ GeV/c for the angular range $2° < \theta < 18°$

In both cases part of the particle identification can be done using time-of-flight measurements, but these will be augmented by Čerenkov measurements. The requirements for the two methods are coupled.

TOF Element	Distance From Vertex	Species Separated	Maximum p (GeV/c) 5σ cut	4σ cut	3σ cut
H1	9 m	π/K	2.9	3.3	3.8
		K/p	5.0	5.7	6.5
H2	20 m	π/K	4.4	5.0	5.8
		K/p	7.4	8.5	9.7
TOFW (midrap.)	4 m	π/K	1.9	2.2	2.5
		K/p	3.3	3.7	4.3

Table 7.1: Dependence of the performance of the various TOF detectors on the cut in number of σ. The value $\sigma = 75$ ps is assumed.

H1

The low momentum PID is done after the dipole D2. At 9 meters from the interaction point the time-of-flight hodoscope H1 can discriminate pions from kaons and protons depending on the time resolution that can be achieved. The expected performance of this detector is listed in Table 7.1. It will consist of 40 staves of size $1 \times 1 \times 25$ cm^3. They will be instrumented by fast photomultipliers mounted at each end, and both time and pulse height information will be read out.

C1

A segmented Čerenkov counter, C1, with C_4F_{10} as radiator gas at 1 atm. can extend the pion identification all the way up to 9 GeV/c, but a gap in the K/p separation will be present between 5.7 (for the 4σ cut) and 9 GeV/c. A segmentation of 8 (two cells along y and four along x) suffices for this counter.

The light collection scheme is shown schematically in Figure 7.1. Each cell is defined optically by a flat mirror angled at 45 degrees to the horizontal and by truncated pyramids which channel the Čerenkov light onto a 3-inch diameter photomultiplier. A prototype of this detector was tested recently[1] and it was found that with a 60 cm radiator length of C_4F_{10} and an RCA8854 photomultiplier, a saturated light yield of some 20 photoelectrons was observed. It was also found during these tests that the background from scintillation was minimal.

The BRAHMS Monte Carlo program was used to evaluate the number of "confusing" events with two particles in one cell. One of those particles has its momentum above threshold and the other below and does not produce any light. The information from this particular cell will then be of no use to extract the identity of the particles because H1 and C1 would not be able to indicate which one of the particles was the one that produced light in the Čerenkov counter. Events with these type of pairs were counted for a setup where the Forward Spectrometer was the closest to the beam, i.e. 2 degrees. The fraction of events with confusing pairs at 2 degrees was found to be equal to 8%, but if the second time-of-flight wall H2 is also taken into account, some of the confused

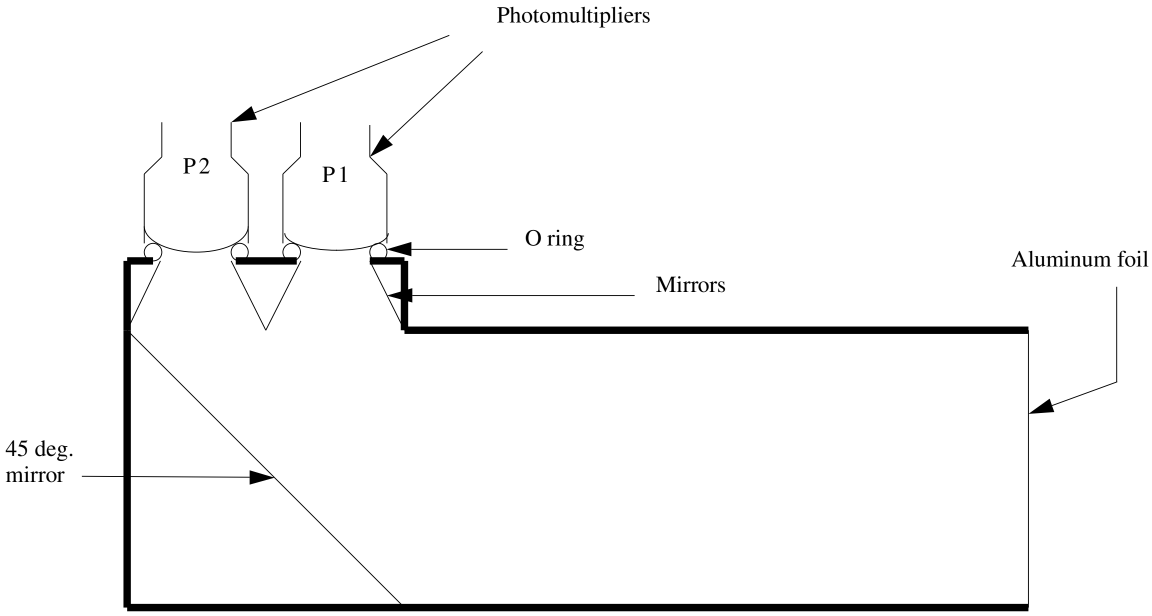

Figure 7.1: Schematic view of the C1 Čerenkov counter. This is a side view, showing how the 45° mirror and photomultipliers P1 and P2 define two cells displaced in the vertical direction.

particles can be identified by time-of-flight, and the fraction of events with unresolved pairs becomes equal to 5%.

H2 and RICH

The high momentum PID will be done with the hodoscope H2, placed 20 meters away from the interaction point and immediately after the tracking detector T5, and with a RICH counter placed after H2. Hodoscope H2, whose performance is listed in Table 7.1, will consist of 20 staves of size $1 \times 2 \times 40$ cm^3, each instrumented by fast photomultipliers mounted at both ends, with time as well as pulse height information read out. The design criteria, expected performance and details of the RICH detector are described below.

Acceptance

The particle identification as done by the different detectors is displayed in Figure 7.2 for the π–K separation and in Figure 7.3 for the K-p separation.

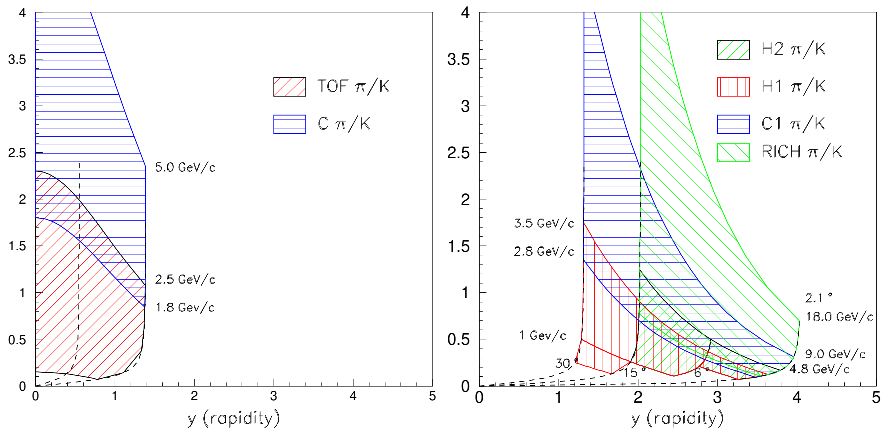

Figure 7.2: Acceptance for pions in the midrapidity (left frame) and forward (right frame) arms. The different shaded areas indicate which detector performs the PID.

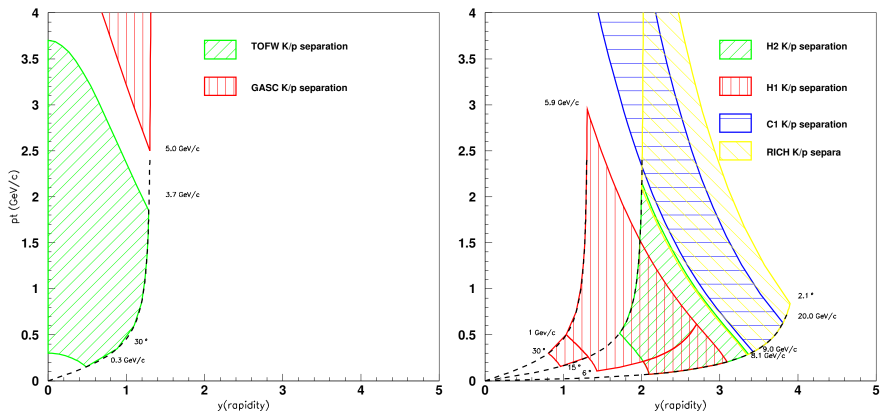

Figure 7.3: Separation of kaons and protons in the midrapidity (left frame) and forward (right frame) arms. The different shaded areas indicate which detector performs the PID.

7.2 Midrapidity spectrometer

The particle identification in the midrapidity spectrometer is designed to be relatively simple. It consists of a time-of-flight wall (TOFW) followed by a segmented threshold Čerenkov detector (GASC), as indicated in Fig. 3.1. The TOFW is 4 meters away from the interaction vetex. With an assumption of 75 ps in overall timing resolution, which is reasonable from recent beam tests, the range of charged hadronic particle separation is given in Table 7.1 under various cut criteria, indicating 4σ separation of K-π up to 2.2

GeV/c and K-p up to 3.7 GeV/c. These momentum ranges contain most of the yield for the particles concerned. However, particles with higher momentum, although few in number, could have different spectrum shapes, revealing unique information on the reaction dynamics.

The GASC detector is proposed to extend the momentum range for particle identification beyond that of TOFW. With Freon-12 gas at 4 atm pressure, pions up to 5 GeV/c, kaons up to 3.7 GeV/c and protons up to 11 GeV/c will be identified. Between 3.7 and 5.0 GeV/c, protons could be contaminated to various degrees by unidentified kaons in the momentum range.

With the center of the midrapidity spectrometer at 34 degrees, the hit probability on TOFW by charged particles, both primary and secondary, is shown in Fig. 6.5, with each TOFW slat 0.6 cm wide and 22 cm high. The calculation is performed for central Au+Au collisions generated by VENUS. The probability is the highest in the middle of the wall and gradually falls down towards both ends. With the same calculation, it is seen that the average multiplicity for charged particles of momentum above the pion threshold (1.6 GeV/c) in the GASC detector is 0.7, posing no special problems for conventional designs of segmented gas Čerenkov counters. A similar, but smaller, design of the successful GASC detector in E-802 at the AGS could be implemented. A segmentation of 20 cells would be more than enough and is very feasible. The segmentation can be achieved optically with flat mirrors and cones for channeling light onto the nearby photomultipliers. In order to make the optical segmentation work correctly, the length of the radiator should be less than 50 cm and the figure of merit N_0 should be close to 90 cm^{-1} in order to get a saturated light yield of some 30 photoelectrons.

7.3 Time-of-flight

Time-of-flight detection is an important part of the BRAHMS particle identification scheme. The forward arm spectrometer uses two time-of-flight walls, H1 and H2, and the midrapidity arm spectrometer uses one, TOFW.

7.3.1 TOFW design

Due to the large multiplicity even in the midrapidity spectrometer at 30 degrees, the TOF wall proposed for the midrapidity spectrometer has to be adequately segmented. Given the present layout of the midrapidity spectrometer, it is desirable to make the individual slats as thin as possible while keeping a reasonable timing resolution ($\leq$ 75 ps). Thinner slats will have less energy deposited by charged particles, and hence larger fluctuations in timing.

We have chosen 22 cm for the height of the TOF wall, and 160 cm for the width. Based on a simulation performed with the midrapidity spectrometer at 34°, the width of the scintillators should be 0.6 cm or smaller.

The proposed arrangement for the phototubes and scintillators on the staves is shown in Fig. 7.4. Light guides direct the photons through a 30° angle to the phototubes at each end. The positions of the light guides are staggered in the assembled wall so as to allow maximum space between neighboring phototubes, as shown in the figure.

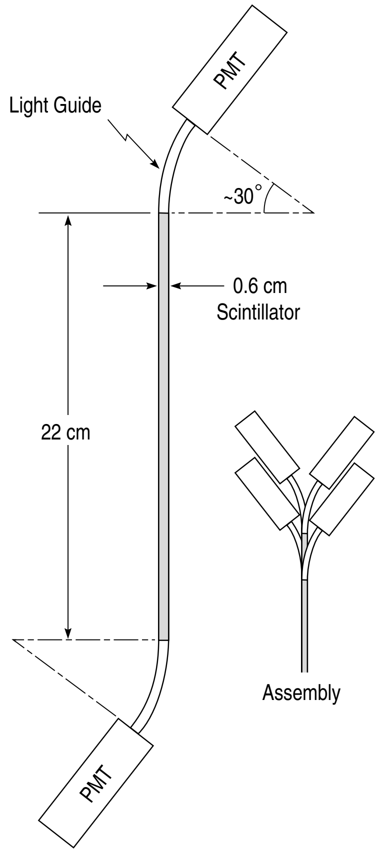

Figure 7.4: Arrangement for mid-rapidity TOF wall staves.

7.3.2 TOF tests

Prototype TOF modules have been studied with the AGS test beam. Two types of scintillators were tested: BC404 $0.6\times0.6\times22$ cm^3 (Type I), and BC404 $0.4\times0.4\times22$ cm^3

Tube	Peak Wavelength (nm)	Rise Time (ns)	Transit Time (ns)	Current (amp)	Price ($)
R1635	420	0.8	7.8	1.0×10^6	427.
R3478S	420	1.3	14.	2.1×10^6	516.

Table 7.2: Characteristics of different phototubes for the TOF.

(Type II). Lucite light guides 6 cm long, matched in cross-section to the scintillator and bent approximately 30 degrees were glued to the end of the scintillators and attached to the phototubes with optical grease. On-Tube-Discriminators from the University of Tsukuba developed for E–866 were connected to the ends of the 3/4-inch phototubes (R3478S) on the Type I scintillator, and a Phillips 8-channel NIM discriminator module was used 50 ft away from the 1 cm tubes (R1635) for the Type II scintillator. Properties of the phototubes tested are given in Table 7.2. The beam particles were mainly 2 GeV/c negative pions. A tiny scintillator (0.5×0.5 cm^2) was placed behind the TOF modules under test and used in conjunction with another 2×2 cm^2 scintillator upstream to define the trigger in order to select beam particles in a small position and angle dispersion. Both ADC's and TDC's were read out by a Macintosh-based data acquisition system.

The timing resolution was analyzed by setting gates of small ranges on the ADC's in order to correct the slewing effect due to the finite rise time of the phototubes. Timing differences between the two tubes on each end of the scintillator, $dt = 0.5 \times (TDC_{up} - TDC_{down})$, were fitted with gaussian distributions, with σ being 61 ps for Type I and 62 ps for Type II. This indicates the timing resolutions for the two types of setup are very similar, in spite of the different scintillator cross-sections, phototubes, and discriminators. The timing resolution between the two scintillators,

$$d(tof) = 0.5 \times (TDC_{up} + TDC_{down})_1 - 0.5 \times (TDC_{up} + TDC_{down})_2 \ ,$$

fits a gaussian distribution with $\sigma = 87$ ps. By assuming both scintillators have the same intrinsic timing resolution, the intrinsic timing resolution for each scintillator is calculated to be $\Delta t = 87/\sqrt{2} = 62$ ps.

In conclusion, intrinsic timing resolution around 60 ps can be achieved by the small scintillators we propose for the BRAHMS Experiment. Depending on the intrinsic timing resolution of the start counters, an overall timing resolution of 70 ps is achievable.

7.4 RICH detector

As described in the PID overview an important part of the high momentum particle identification is performed by a RICH (Ring Imaging CHerenkov) detector. RICH counters are powerful tools for achieving particle identification over a wide range of momentum within a single detector. The experience of the SLD[2] and DELPHI[3] Collaborations in developing broad-range detectors has shown that π/K/p separation can be achieved up to approximately 30 GeV/c and e/π separation can be performed up to 5 GeV/c. There is also the capability of handling modest multiplicities within the detector. For reviews on the subject, see Refs. 4 and 5.

For a given particle the frequency distribution of Čerenkov radiation, $dN/d\nu$, is constant for all frequencies, ν, leading to several possible photon detection schemes. Existing RICH counters generally detect the Čerenkov photons in the UV region (6.5 – 7.5 eV) by means of photoionization of a complex organic molecule, such as TMAE or TEA, in a proportional gas chamber. Alternatively, a segmented optical readout based on an array of photomultipliers offers three main advantages over the gas-based drift chamber:

1. No special handling for hazardous materials such as TMAE.
2. The possibility of readout fast enough for first-level triggering.
3. Greater overall efficiency due to larger bandwidth (2.5–4.3 eV).

As shown in Fig 3.1 the time-of-flight wall H2 is at a distance of 20 m from the vertex. At the 3σ level (where $\sigma = 75$ ps) it separates π/K up to $p = 5.8$ GeV/c and K/p up to $p = 9.7$ GeV/c (see Table 7.1). Using the criterion that two decades of coverage in the inclusive invariant cross-section are required, the RICH detector must separate π/K up to 20 GeV/c and K/p up to $\approx$30 GeV/c at the 2° polar angle setting (see Chapter 3).

For the RICH counter, located just behind H2, it is proposed to have 1.5 m of C_4F_{10} radiator at 1.25 atmosphere pressure ($n = 1.00185$). This choice of radiator allows overlap of coverage with the TOF system and determines the resolution in ring radius, $\Delta r/r$, required to obtain the desired momentum coverage. The Čerenkov photons are focused by a spherical primary mirror with radius of curvature $R = 3.0$ m (i.e. focal length $f = 1.5$ m) onto the focal-plane. The photons are detected by four segmented 10×10 cm^2 multi-anode photomultipliers arranged in a tightly packed manner. Each photomultiplier comprises a subarray of $10\times10=100$ pixels (each 1 cm^2 in area), representing a total segmentation of 400 pixels. The trajectories of the incoming charged particles will be known from the tracking in the Forward Spectrometer, and thus the position of the center of each Čerenkov ring may be deduced. In addition, the momentum of each tracked particle is also measured; thus it is sufficient to discriminate between known ring radii in order to perform the π/K/p particle identification.

It is important to note that the expected multiplicity of charged particles through the RICH counter is low. This has been confirmed by GEANT simulations of several hundred events generated by Venus and tracked through the BRAHMS Forward Spectrometer. Only particles which entered through the front-face of the spectrometer were tracked; thus the analysis was not concerned with background particles generated, for example, in the beampipe or the air. The RICH detector is far enough away from the beampipe that this is likely not a concern. The estimated multiplicities are given in Table 7.3.

	Hits per event p=7.5-15 GeV/c	Hits per event p=15-30 GeV/c
Primary	0.9	0.29
Secondary	0.5	0.39
Above threshold	0.8	0.30

Table 7.3: Average charged particle hits in the RICH detector

As can be seen from the table the proposed RICH counter will have to deal with at most a few particles per event. Typically, the tracks will be separated in angle by $\sim$2.0° in the bend plane and $\sim$0.5° in the non-bend plane which leads to a displacement of the ring center of $\sim$1 cm, enough to distinguish the individual particles.

Arrays of single-anode PMT's have been used successfully in previous RICH counters[7], but state-of-the-art multi-anode PMT's offer the advantage of many channels with a single common power supply and a compact readout. A working prototype counter has performed well in the AGS test beam and proven the multi-anode PMT technique (see Appendix A.)

7.4.1 Design Requirements and Detector Performance

The principal features of a RICH detector satisfying the design considerations outlined above are shown in Fig. 7.5. The radiator volume is filled with C_4F_{10} which, at a temperature of 20°C and 1.25 atm pressure has an index of refraction of n=1.00185. Reaction products π, K and p emerging from the exit aperture of D4 (h$\times$w=40 cm$\times$50 cm) pass through the volume, entering and exiting via the aluminum-alloy windows ($<$ 250 mg/cm^2). Čerenkov radiation produced along the 1.5 m path length (i.e. before the mirror) is focused by the spherical concave mirror (focal length f = 1.5 m) on the focal-plane detector as shown. The mirror itself has been rotated by an angle α = 8° about a horizontal axis through its center, thus shifting the ring image by an angle 2α = 16°. This places the ring image outside the radiator volume so that the primary particle flux cannot produce Čerenkov light in the glass walls of the photomultipliers.

Before proceeding to further discussion of the reason for various design features, it should be emphasized that the design illustrated can be constructed with components presently available. Key elements of the design, specifically the photon imaging detector, mirror and radiator gas, have been successfully tested in beam using the prototype RICH detector of BNL RD-44 with runs in 1992, 1993 and 1994. (For details see Appendix A.)

The focal plane detector consists of four Hamamatsu H-4945 multianode photomultipliers situated as indicated in Fig. 7.5. Each PMT consists of a 10$\times$10 array of 1

cm^2 pixels mounted in a glass envelope of 12.8×12.8 cm^2 outside dimensions. Thus the outside dimensions of the focal-plane detector system are 25.6×25.6 cm^2 and the active area measures 22.8×22.8 cm^2 with a central dead region resembling a cross, as shown, of about 2.8 pixels in width. A vacuum seal on the four phototubes is used to constrain the radiator gas to the interior of the RICH vessel.

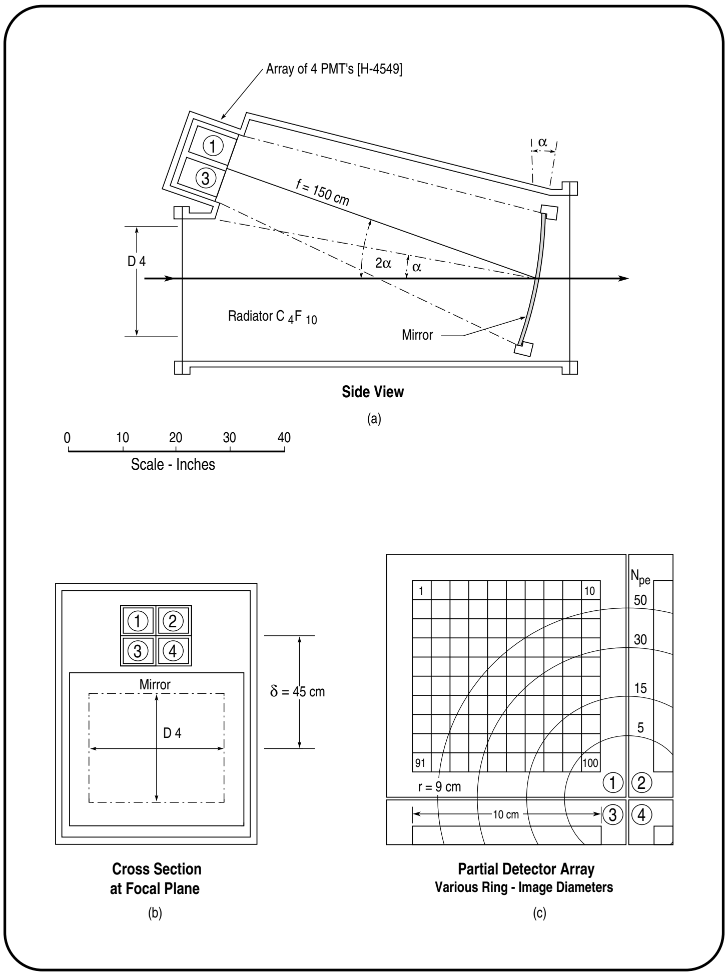

Figure 7.5: Schematic outline of RICH detector

Performance Characteristics

<u>General</u>

For a charged particle of velocity $\beta = v/c$ travelling through a medium with index of refraction n, the Čerenkov angle for photon emission is given by

$$\theta = \cos^{-1}(1/\beta n) \ .$$

The radius of the ring-image at the detector focal plane is $r = f \tan\theta$. The number of detected photons may be written as[9]

$$N_{detected} = N_0 \, L \, \sin^2\theta \ ,$$

where L is the pathlength, in cm, and N_0 is the quality parameter of the counter, which is related to the integral over the photon energy, E, of the detector quantum efficiency $\epsilon(E)$ by:

$$N_0 = 370 \ (\text{cm eV})^{-1} \, \epsilon_m \int \epsilon(E) \, dE,$$

where ϵ_m is the reflection efficiency of the spherical mirror = 90%. For the Hamamatsu detector H-4549, the integral of $\epsilon(E)$ over E has the value 0.33 eV, and thus N_0=110 cm^{-1}.

Figure 7.6 shows plots of the ring radius, r, versus particle momentum, p, for pions, kaons and protons. Panel (a) uses the value N_0=110 cm^{-1} given above, while panel (b) assumes, as a worst case, the value N_0=55 cm^{-1}. Confidence contours at the 3σ level are included, where $\sigma = 0.0505/\sqrt{N_{pe}}$ and N_{pe} is the mean number of detected photoelectrons (see discussion below.) Also illustrated are the 3σ limits for π-K and K-p separation by the time-of-flight hodoscope H2. Even for the pessimistic N_0=55 cm^{-1} case, the RICH counter is expected to extend the particle identification from H2 to >20 GeV/c for π-K and to >35 GeV/c for K-p.

The right-hand scales of Fig. 7.6 show the expected mean number of detected photons for rings of different radii. The first column of numbers assumes the full detector coverage over the focal plane. The numbers in parentheses are acceptance-corrected for the inactive region as shown in Fig 7.5.

Detector Resolution: Aberrations and Pixel Size

It is evident from Fig 7.6 that the most stringent test of the detector resolution occurs in the momentum range p=20–30 GeV/c where it is essential to distinguish, on the basis of the measured ring radius r, the character of the particle as a pion or a kaon. In the following, it should be remembered that since $\theta = \cos^{-1}(1/\beta n) \leq 0.006$ rad $\ll 1$, we have $\tan\,\theta \approx \theta$ and thus the relationship between θ and r is $\theta = r/f$. This implies that the fractional uncertainties $\Delta\theta/\theta$ and $\Delta r/r$ are equal within negligible errors. The center of the ring distribution, in conjunction with the tracking information, is accurately determined. The uncertainty in an *individual* photoelectron hit position can be written as

$$\left(\frac{\Delta\theta}{\theta}\right)^2 = \left(\frac{\Delta\theta}{\theta}\right)^2_{\text{chromatic}} + \left(\frac{\Delta\theta}{\theta}\right)^2_{\text{geom}} + \left(\frac{s}{r\sqrt{12}}\right)^2 .$$

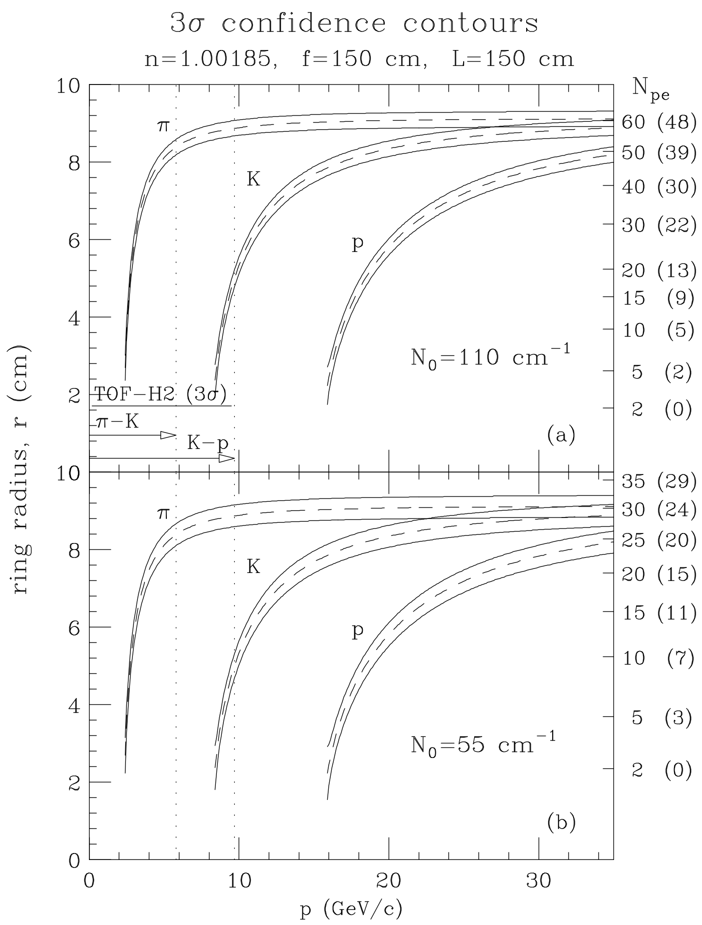

Figure 7.6: Ring radius and number of photoelectrons versus momentum. The number of photoelectrons given in parentheses are for the active area only.

The first two terms on the right express, in order, the effect of chromatic and geometric (optical) aberrations; the last term accounts for the finite pixel size, s, with the factor $\sqrt{12}$ arising from the r.m.s. error on the radius from assuming the position of the center of the pixel. We now evaluate these terms in the high momentum limit of β=1 for the parameters specified above and in Fig 7.6a.

Aberrations

The chromatic aberration is irreducible, in the sense that it follows directly from the choice of radiator gas. In a C_4F_{10} radiator at 1.25 atmosphere, the chromatic aberration is calculated[9] to be

$$\left(\frac{\Delta\theta}{\theta}\right)_{\text{chromatic}} \approx \frac{1}{2}\frac{\Delta n}{n-1} = 0.0315 \ .$$

In the above $\Delta n/(n-1)$ is simply the fractional change in the index of refraction over the 1.8 eV bandwidth of the photon detector.

The geometric aberration depends on the details of the RICH detector geometry, particularly on the ratio $x = \delta/R$, where R is the radius of curvature of the spherical mirror and δ is the perpendicular displacement of the focal plane detector from the particle trajectory axis. The geometric aberration is given by:

$$\left(\frac{\Delta\theta}{\theta}\right)_{\text{geom.}} = \left\{(n-1)\sqrt{3} \oplus \frac{\sqrt{42(n-1)}}{7} \cdot x \oplus x^2\right\} = 0.0235 \ ,$$

where $\oplus$ indicates addition in quadrature. Here we have used the case of a particle trajectory passing through the center of the spherical mirror shown in Fig. 7.5; thus $\delta = f \sin 2\alpha \approx 45$ cm, with the resulting value x=45/300=0.15. The x^2 term clearly dominates the expression for $\Delta\theta/\theta$.

Pixel Size

The last term specifies the fractional contribution to the net uncertainty (for a single hit) due to the fact that the pixel size, s, may represent a significant fraction of the ring radius, r. For fully relativistic particles the ring radius is 9.1 cm, compared to the pixel dimension of 1 cm, and thus

$$\left(\frac{s}{r\sqrt{12}}\right) = 0.0317$$

.

Net resolution

Combining the results for β=1 particles, such as 25 GeV/c pions, we compute the fractional uncertainty

$$\frac{\Delta\theta_\pi}{\theta_\pi} = \sqrt{.00255} = 0.0505$$

or $\Delta\theta_\pi = \theta_\pi \times 0.0505 = 0.00306$.

A figure of merit for distinguishing π from K may now be written as

$$n_\sigma = \frac{\theta_\pi - \theta_K}{\sqrt{\Delta\theta^2/N'_{pe}}} \ ,$$

where n_σ is the number of standard deviations separating π from K. Here N'_{pe} is the minimum number of detected detected photons, which is taken as $N'_{pe} = N_{pe} - 2\sqrt{N_{pe}}$.

From Fig 7.6a with p=25 GeV/c, N_{pe} =48 implying N'_{pe}=34, and finally

$$n_\sigma = 6.5 ,$$

i.e., the determined radius is more than six standard deviations away from what might be expected from a kaon.

7.4.2 Expected performance

Simulated images of Čerenkov rings on the focal-plane of the RICH detector are shown in Fig. 7.7. Panel (a) shows that a high momentum (18 GeV/c) pion may be discriminated from a kaon or proton by the observed ring radius. The ring from a 10 GeV/c kaon is also easily seen (in Fig. 7.7b) despite the dead space between the photomultiplier tubes. Finally, Fig. 7.7c shows two overlapping pion rings which may be readily separated and identified.

In order to understand better the real pattern of rings expected behind the forward spectrometer, Monte Carlo simulations were performed. Central Au+Au events produced by Venus were run through the forward spectrometer with the code GEANT, and the RICH rings, if any, from primary and secondary (background) particles were then generated. Fig. 7.8 summarizes a key feature of the results, namely the distribution of the ring centers in the focal plane. Fig. 7.8a shows that the positions of the ring centers from "good" primary particles are concentrated in a narrow horizontal band (along the bend-plane of the spectrometer magnets) at the center of the acceptance. Ring centers from background secondary particles, however, are scattered more or less randomly throughout the acceptance, as seen in Fig. 7.8b. This fact greatly aids in reconstructing the good rings since the background rings generally do not appear fully in the active area of the focal-plane.

The event ring patterns output by the Monte Carlo calculation were visually scanned in order to determine the reconstruction efficiency. In a study of 100 events with the forward spectrometer at the 2 degree, 7.5-15 GeV/c setting and with the RICH parameters set at (the not quite final values of) n = 1.00175, N_0 = 100 cm^{-1}, L = 100 cm and f = 150 cm, all the rings of 96 events were successfully found and identified. Since random "noise hits" were not included in the simulation, it is important to prove that we have conservatively designed the RICH counter in terms of the photon yield. To this end, a separate Monte Carlo run was performed with the quantum efficiency at half the expected value, i.e., with N_0 = 50 cm^{-1}. In this case the ring reconstruction efficiency found by visual scanning was almost unchanged: 93/100 of the events were complete successes.

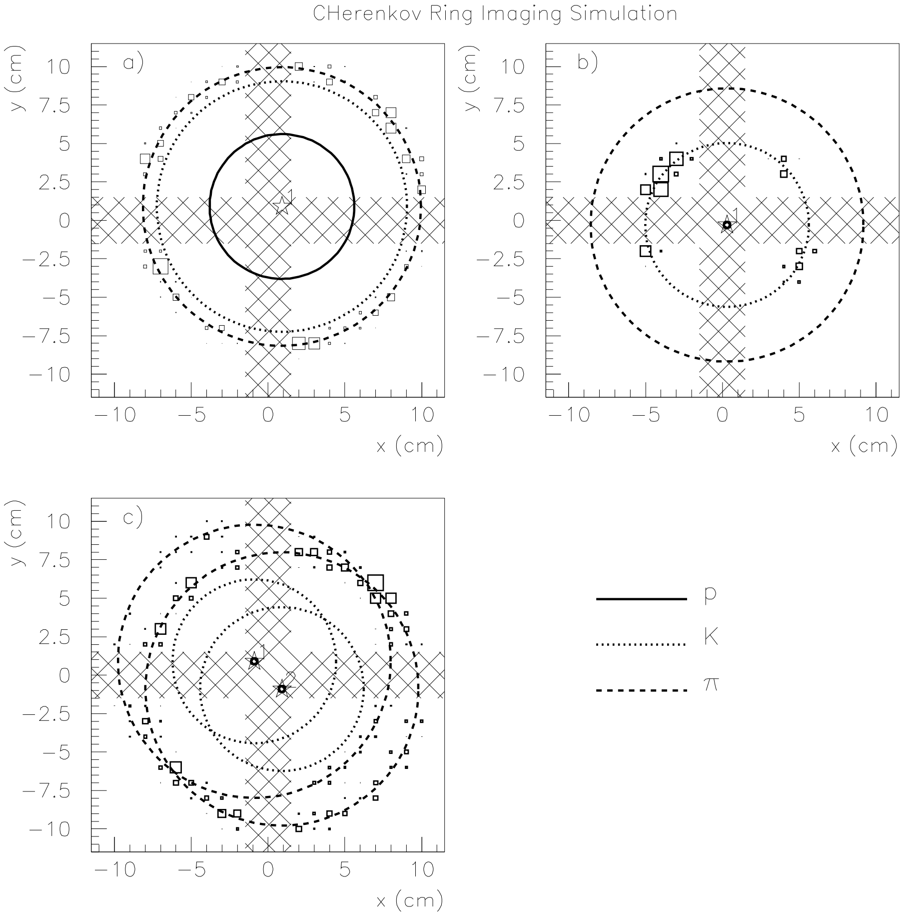

Figure 7.7: Simulated ring patterns for the RICH detector focal-plane with $n = 1.00185$, $N_0 = 110\ \mathrm{cm}^{-1}$, $L = 150$ cm and $f = 150$ cm. The sizes of the boxes indicate the pulse height on active pixels ($1 \times 1\ \mathrm{cm}^2$ each) with the cross-hatched area being dead. Independent tracking yields the ring centers (stars) and momenta, which imply the drawn circles for different particle species. Panel a shows an 18 GeV/c pion, panel b shows a 10 GeV/c kaon, and panel c shows two 10 GeV/c pions.

7.5 References

1. R. Debbe, et al., Report on tests of detector prototypes for the extended PID of E866, internal E866 memo E-866-MEM-10, 1994.
2. V. Ashford, et al., presented at the XXIII Int. Conf. on High Energy Physics (Berkeley, CA, July 16–23, 1986) SLAC-PUB-4046; V. Ashford, et al., IEEE Trans. Nucl. Sci. **NS-34**, 499 (1987).
3. DELPHI Collaboration, Nucl. Instrum. and Meth. **A303**, 233 (1991).
4. T. Ypsilantis, Proc. of the Symposium on Particle Identification at High Luminosity Hadron Colliders, T. J. Gourlay and J. G. Mofin, ed., Fermilab, p. 133

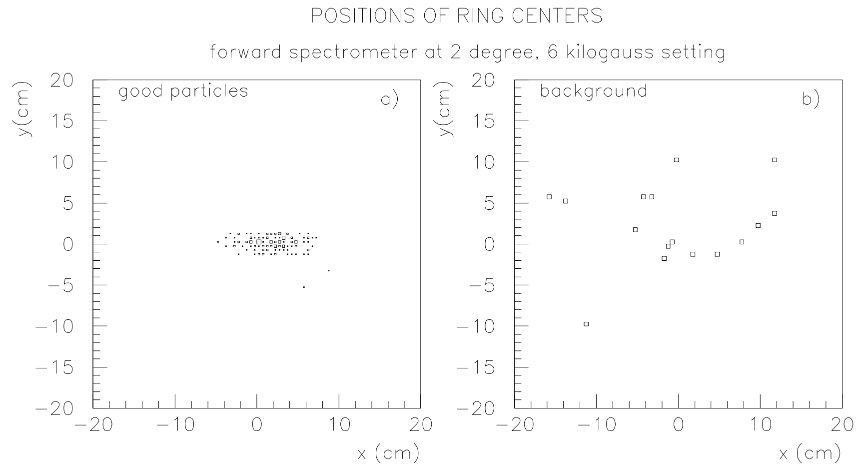

Figure 7.8: Position of the ring centers for good primary particles (panel a) and for secondary background tracks (panel b) from a GEANT simulation of 145 Venus central Au+Au events through the BRAHMS forward spectrometer at the 2 degree, 7.5-15 GeV/c setting.

(1989).

5. D. Leith, Nucl. Instrum. and Meth. **A265**, 120 (1988).
6. T. Sugitate, et al., Nucl. Instrum. and Meth., **A307**, 265 (1991); S. Endo, et al., "A Test of an Improved RICH Prototype", Institute for Nuclear Study (Tokyo) Annual Report, 1990.
7. See, e.g., Proc. of the Seminar held on the Occasion of the 50th Anniversary of the Discovery of Vavilov-Čerenkov Radiation, P. Carlson, ed., Nucl. Instrum. and Meth. **A248** (1986).
8. D. Beavis, et al., RHIC Letter of Intent #8, Brookhaven National Laboratory, 1990; Addendum to RHIC Letter of Intent #8, Brookhaven National Laboratory, 1991.
9. T. Ekelof, "The Experimental Method of Ring-Imaging Cherenkov (RICH) Counters", lecture given at the 1984 SLAC Institute on Particle Physics, 23 July–3 August 1984, CERN-EP/84-168.